Vol. **113** (2008) *ACTA PHYSICA POLONICA A* No. 2

Stokes Shift and Band Gap Bowing in $In_xGa_{1-x}N$ ($0.060 \leq x \leq 0.105$) Grown by Metalorganic Vapour Phase Epitaxy

A. Yildiz[a,*], F. Dagdelen[b], S. Acar[c], S.B. Lisesivdin[c], M. Kasap[c], Y. Aydogdu[b] and M. Bosi[d]

[a]Department of Physics, Faculty of Science and Arts
Ahi Evran University, Asikpasa Kampusu, 40040 Kirsehir, Turkey
[b]Department of Physics, Faculty of Science and Arts
Firat University, 23169 Elazig, Turkey
[c]Department of Physics, Faculty of Science and Arts
University of Gazi, Teknikokular, 06500 Ankara, Turkey
[d]CNR-IMEM Institute, Area delle Science 37/A
43010 Fontanini, Parma, Italy

(Received July 16, 2007; in final form December 7, 2007)

We presented the results of electrical and optical studies of the properties of $In_xGa_{1-x}N$ epitaxial layers ($0.060 \leq x \leq 0.105$) grown by metalorganic vapour phase epitaxy. Resistivity and Hall effect measurements of the samples were carried out at room temperature. Optical properties of the samples were characterized by photoluminescence and optical absorption spectroscopy. The comparison between the photoluminescence and the optical absorption measurements gives the Stokes shift. We explained the observed Stokes shift in terms of Burstein–Moss effect. The band gap versus composition plot for $In_xGa_{1-x}N$ alloys is well fitted with a bowing parameter of ≈ 3.6 eV.

PACS numbers: 73.61.−r, 78.20.−e, 78.40.Fy, 78.55.−m

1. Introduction

$In_xGa_{1-x}N$ alloy system has received a great deal of interest due to an important number of applications such as light emitting diodes [1], laser diodes [2],

*corresponding author; e-mail: yildizab@gazi.edu.tr

visible blind photodetectors [3], and heterostructure field effect transistors [4]. For these applications, it is important to investigate the material's band gap as a function of its composition. Also, this investigation performs to design new device structures.

In order to determine the luminescence activity of $In_xGa_{1-x}N$, it is necessary to know its optical properties. There have been many efforts to determine optical properties of $In_xGa_{1-x}N$ using various spectroscopic techniques [5–7]. Studies of the optical properties of Ga-rich $In_xGa_{1-x}N$ have shown a strong dependence of the fundamental band gap on the alloy composition. It is accompanied by a large band gap bowing and giant Stokes shift between the photoluminescence (PL) peaks and the optical absorption (OA) edges. In order to explain this energy shift, one of possible mechanisms is the phase separation. It has been reported that indium segregation mechanism is important in thick InGaN layers. Originating from the phase separated In-rich region plays a significant role in the emission mechanism of nitride-based LEDs [8]. Although, there have been several publications giving $In_xGa_{1-x}N$ band gap information, they show a significant dispersion with values for the bowing parameter ranging from 1 eV [9] to 5.9 eV [10]. This may be due to experimental difficulties related to the method used to measure optical gap. Since the lattice mismatch is large between GaN and InN, the epitaxial growth of InGaN on GaN leads to strains in the InGaN layer. Strain also has an important effect on the band structure in $In_xGa_{1-x}N$ [11]. This effect increases with increasing indium composition in $In_xGa_{1-x}N$. It can result in a large Stokes shift observation. In the case of a degenerate semiconductor, this Stokes shift can also closely correlate with an increase in free electron concentration.

In this work we reported a study on the electrical and optical properties of $In_xGa_{1-x}N$ epitaxial layers ($0.060 \leq x \leq 0.105$) grown by metalorganic vapour phase epitaxy (MOVPE). Resistivity and Hall measurements were performed on every sample at room temperature. The PL and the OA properties are also investigated at room temperature. The emission spectrum of the $In_xGa_{1-x}N$ system extends to visible red. The bowing of band gap had been derived from the OA measurements.

2. Experimental

The InGaN epilayers presented in this work were grown in an atmospheric pressure vertical MOVPE reactor with a shower head configuration. Standard ammonia, trimethylgallium (TMGa), and trimethylindium (TMIn) precursors were employed, while N_2 was always used as main carrier gas. However, H_2 was also introduced into the reactor through two channels: first, it was always used as carrier gas for the alkyls and, second, in controlled amounts via an additional make-upline. This allowed for an investigation about the role of the overall H_2 partial pressure in controlling the In incorporation. The TMGa precursor was delivered to the reactor via a double-dilution line, which allows changing the Ga molar fraction

while maintaining constant the hydrogen flow injected into the growth chamber. The TMIn was instead introduced via a standard single-dilution line, where a given hydrogen flow enters into the bubbler and drags a quantity of TMIn dependent on the temperature and the bubbler pressure controlled, respectively, by a thermostatic bath and an on-line pressure controller. Obviously, with this system the TMIn molar fraction delivered to the growth chamber is always proportional to the hydrogen flow. The 2″ sapphire substrates were rotated around their axis at rates varying between 120 and 750 rpm: the change in rotation speed allowed controlling the growth rate, which has a strong influence in indium content in the alloy as reported previously [12, 13]. The standard heterostructure included a 80–100 nm thick GaN buffer grown at 510°C, a 600 nm thick GaN layer deposited at 1080°C (a typical V/III ratio was about 7000), and an InGaN alloy deposited at 800°C with different conditions, as reported above, in order to vary In content.

The high-resolution X-ray diffraction (HRXRD) measurements were performed by using a D8/Bruker diffractometer, equipped with a Cu source and a Ge (022) monochromator. The In composition was determined by HRXRD assuming that the lattice parameter varies linearly with the In fraction according to Vegard's law. The obtained In composition values are in excellent agreement as reported previously [12]. The thickness of the InGaN epilayers was approximately 600 nm with indium composition varying from 0.060 to 0.105.

For the resistivity and Hall effect measurements by the van der Pauw method, square-shaped (5×5 mm^2) samples were prepared with four contacts at the corners. Using either evaporated or annealed indium dots, ohmic contacts to the samples were prepared and their ohmic behaviour was confirmed by the current voltage characteristics. The measurements were made at room temperature using a Lakeshore Hall effect measurement system (HMS). The magnitude of the magnetic field was 0.5 T.

The samples were also characterized by the PL and the OA spectroscopy. All optical measurements were performed at room temperature. A 55 mW He–Cd laser (325 nm) is used as a light source in room temperature PL measurements. The OA measurements were recorded using a Perkin Elmer 45 UV+VIS spectrophotometer, in the wavelength range from 200 to 1100 nm.

3. Results and discussion

In order to investigate electrical properties, resistivity and Hall measurements were performed on every sample at room temperature. For the studied samples, Hall measurements indicated n-type behaviour, which may be due to the presence of nitrogen vacancies. The results of the Hall measurements were given in Table. It can be seen from Table that the mobility μ in $In_xGa_{1-x}N$ samples is lower than the one in GaN, which is usually more than 400 cm^2 V^{-1} s^{-1} at room temperature. This behaviour suggests that the more indium is added to alloy, the more scattering centres are created and it should result in low mobility.

TABLE

Experimental results of Hall, PL, and OA measurements at room temperature.

x	Hall results			PL results		OA results
	μ $[\frac{\mathrm{cm}^2}{\mathrm{Vs}}]$	n $[10^{18}\ \mathrm{cm}^{-3}]$	ρ [Ω cm]	Gaussian peaks [eV]	Line [meV]	E_g [eV]
0.060	40.6	28.5	0.0052	2.935; *3.074*	153	3.08
0.085	22.5	7.51	0.0369	2.331; *2.687*; 2.947	317	2.90
0.105	15.5	5.44	0.0746	2.299; *2.567*; 2.851	282	2.82

We can see that the Hall carrier concentrations decrease with increasing indium composition (x), while the resistivity increases. For $In_xGa_{1-x}N$ samples, measured carrier concentrations are above the critical Mott density ($n_c^{1/3}a_H^* = 0.25$) [14], where n_c and a_H^* are critical carrier concentration and the effective Bohr radius, respectively. With these carrier concentrations, $In_xGa_{1-x}N$ exhibits degenerate semiconductor behaviour. Above the Mott density, for the case of n-type doping, the Fermi level is slightly higher than the conduction band bottom. The band gap can then be larger or smaller. The widening that occurs in $In_xGa_{1-x}N$ is due to the lowest states of the conduction band that are blocked; this is the well-known Burstein–Moss effect [15, 16]. We observed that band gap of $In_xGa_{1-x}N$ is wider with increasing carrier density. Later we will discuss Burstein–Moss effect in relation to band filling, on other properties of $In_xGa_{1-x}N$.

Figure 1 shows the room temperature PL spectra of the InGaN layers. The main PL peaks were located between 360 and 640 nm with intensities dramatically

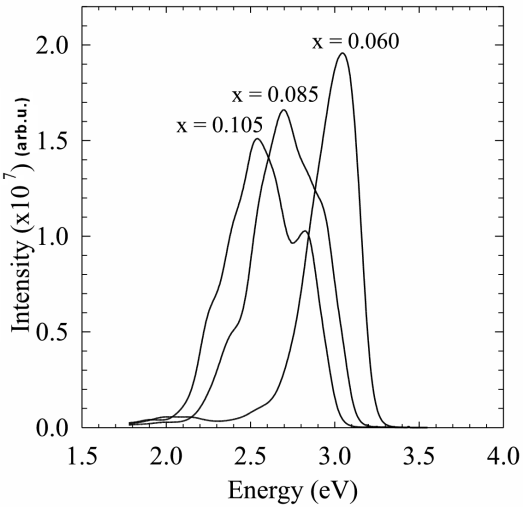

Fig. 1. Room-temperature photoluminescence spectra of $In_xGa_{1-x}N$ for $x = 0.060$, $x = 0.085$, and $x = 0.105$.

different among samples. In order to determine the peak position and the line width of the emission components, each PL spectrum was fitted by a Gaussian distribution function. A single Gaussian peak did not accurately describe our PL spectrum. We observed two or three emission peaks in all of the PL spectra, shown in Fig. 1. The peak positions were thus determined by fitting two or three overlapping Gaussians to the luminescence peak. The peak positions of the higher energy component and lower energy components were shown in Table. The line widths of higher energy components accepted as band gap were also shown in Table. The band gap values obtained from the PL measurements were of the same order of magnitude as found in variety of InGaN systems [17–20]. However, our linewidth values are somewhat higher compared with reported values in literature. InGaN alloys are thought to be thermodynamically unstable even for moderate indium composition ($x \geq 0.060$) [21]. Therefore, there is observed compositional inhomogeneity or strain and it should result in high line width values in $In_xGa_{1-x}N$ layers. Due to the presence of strain in InGaN samples, our line width values were slightly higher than reported values by several researches [22, 23]. Also, lattice mismatch between GaN and sapphire substrate are sufficient to generate misfit dislocations. Finally, effects of the lattice mismatch result in degrading the luminescence efficiency of the InGaN alloys [24].

We can conclude with considering the whole PL spectra that the line width of the PL peak is significantly broadened and PL spectra shift regularly along the increasing wave length (to visible red), as indium composition increases. Actually, the quality of the samples becomes better while the indium composition (x) decreased as indicated by the changes of the line width.

The analysis of optical absorption spectra is one of the most productive tools for understanding and developing the band structure and energy gap of materials [25]. In this connection, the OA of InGaN samples is measured.

The relationship between absorption coefficient and optical band gap is expressed by the following equation [26]:

$$(\alpha h\nu)^2 = B\,(h\nu - E_{\mathrm{g}})\,, \tag{1}$$

where B is a parameter that depends on the transition probability, $h\nu$ is the incident photon energy, and E_{g} is the band gap of the material. The optical band gap was determined from the plots of $(\alpha h\nu)^2$ vs. $h\nu$ (Fig. 2). Extrapolating the linear part of each plot towards lower photon energies, the point of interception with the $h\nu$ axis exists at $(\alpha h\nu)^2 = 0$ giving the corresponding band gap. The estimated band gap energies were shown in Table. The band gap values obtained from the OA measurements were of the same order of magnitude as found in variety of InGaN systems reported by many researches with the OA measurements [18, 21, 27].

The band gaps determined from the absorption edges in Fig. 2 were shown as a function of indium composition in Fig. 3. The absorption edge shifts to lower energy as x increases. As shown by the solid curve in Fig. 3, the indium com-

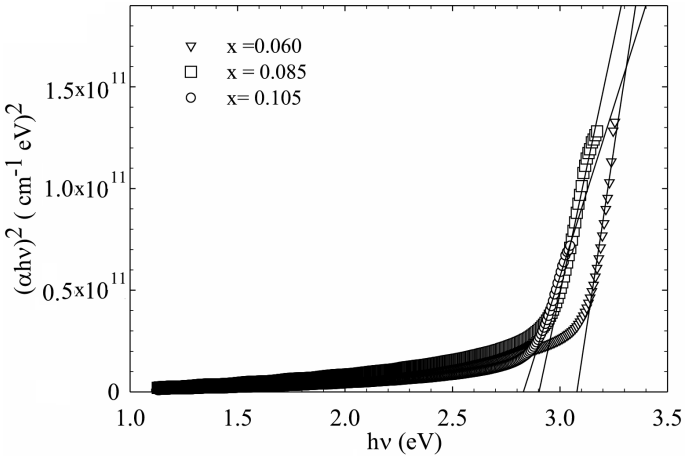

Fig. 2. The plot of $(\alpha h\nu)^2$ versus photon energy of $In_xGa_{1-x}N$ layers.

position dependence of the room temperature band gap in the entire composition range can be well fitted by the following standard equation:

$$E_{\mathrm{InGaN}}(x) = (1-x)E_{\mathrm{GaN}} + xE_{\mathrm{InN}} - bx(1-x), \tag{2}$$

where $E_{\mathrm{InGaN}}(x)$ represents the band gap energy of $In_xGa_{1-x}N$ and E_{GaN}, E_{InN} are the band gaps of GaN and InN, respectively, and b is the optical bowing parameter [2]. The curve fitting for the OA edge energies was carried out with $E_{\mathrm{InN}} = 0.8$ eV, $E_{\mathrm{GaN}} = 3.42$ eV and then the best fit was achieved with $b = 3.6$ eV as shown by the solid line in Fig. 3. It is reported a strong gap bowing, from both experimentally and first principles calculations, with values ranging from 2.6 eV to 5.9 eV by many researches [5, 10] for indium composition $x < 0.25$ in $In_xGa_{1-x}N$. The large value and strong composition dependence of the bowing parameter can be attributed to strain within the structure.

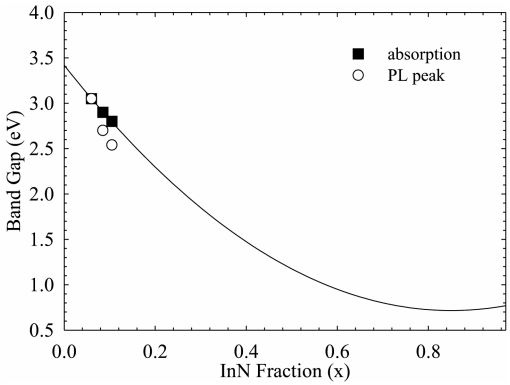

Fig. 3. In-composition dependences of PL energy and absorption edge of $In_xGa_{1-x}N$. The solid line shows the fit to the band gaps using Eq. (2).

The indium composition dependence of the peak energy of the PL signal was also shown in Fig. 3. Our measured values of the band gap were somewhat lower than the ones obtained by OA. This difference is to be expected, since the PL peak energies of thick InGaN layers are typically lower than the band gap energies [28]. The comparison between the OA and the PL allows determining the Stokes shift. The Stokes shift of the strong peak energy components which are written as italics in Table, is estimated to be 6 meV for $x = 0.060$, 213 meV for $x = 0.085$, and 253 meV for $x = 0.105$, respectively. The Stokes shift increases with an increase in indium composition. The reason for the Stokes shift in InGaN samples was explained by many researchers with defects [21], strains [20], alloy fluctuations [8], piezoelectric fields [29], phase-separation [18] as well as band filling effect (Burstein–Moss effect) [30]. In our case, the InGaN samples exhibited a degenerate semiconductor behaviour. In a degenerate semiconductor, the band-edge emission energy in PL measurements is expected to shift toward higher energies for increasing carrier concentration due to the change of the Fermi level (Burstein–Moss effect) [2]. We obtained that the carrier concentration increases with decreasing indium composition and the PL spectra shifted toward higher energies in our degenerate InGaN samples. The Stokes shift can thus be in a large part explained by this effect. However, the Burstein–Moss effect does not exceed a few tens of meV. Therefore, it should be a considered effect of strain in thisgiant Stokes shift.

4. Conclusion

We have investigated electrical and optical properties of $In_xGa_{1-x}N$ epitaxial layers ($0.060 \leq x \leq 0.105$) grown by MOVPE as a function of indium composition as well as carrier concentration, using the Hall effect, the PL and the OA spectroscopy. We obtained the Stokes shift with the comparison between the PL and the OA. From the Hall measurement, it was assumed that all samples have a degenerate semiconductor behaviour. Then the Stokes shift was explained in terms of the Burstein–Moss effect as well as the contribution of strains. The bowing of band gap was derived from the OA measurements. It was found that there was a strong bowing effect on the band gap. Our experimental results suggested that the bowing parameter for $In_xGa_{1-x}N$ was approximately 3.6 eV in the composition range between $x = 0.060$ and $x = 0.105$.

Acknowledgments

This work is supported by the State of Planning Organization of Turkey under grant No. 2001K120590.

References

[1] T. Mukai, K. Takekawa, S. Nakamura, *Jpn. J. Appl. Phys.* **37**, L839 (1998).

[2] S. Nakamura, G. Fasol, *The Blue Laser Diode*, Springer, Berlin 1997, p. 133.

[3] Y.K. Su, C.Y. Zung, F.S. Juang, S.J. Chang, J.K. Sheu, *Jpn. J. Appl. Phys.* **40**, 2996 (2001).

[4] G. Simin, X. Hu, A. Tarakji, J. Zhang, A. Koudymov, S. Saygi, J. Yang, A. Khan, M.S. Shur, R. Gaska, *Jpn. J. Appl. Phys.* **40**, L1142 (2001).

[5] M.D. McCluskey, C.G. Van de Walle, C.P. Master, L.T. Romano, N.M. Johnson, *Appl. Phys. Lett.* **72**, 2725 (1998).

[6] T. Ohashi, T. Kouno, M. Kawai, A. Kikuchi, K. Kishino, *Phys. Status Solidi A* **201**, 2850 (2004).

[7] L.H. Robins, A.J. Paul, C.A. Parker, J.C. Roberts, S.M. Bedair, E.L. Piner, N.A. El-Masry, *MRS Internet J. Nitride Semicond. Res.* **4S1**, G3.22 (1999).

[8] S. Chichibu, T. Azuhata, T. Sota, S. Nakamura, *Appl. Phys. Lett.* **70**, 2822 (1997).

[9] S. Nakamura, N. Iwasa, S. Nagahama, *Jpn. J. Appl. Phys.* **32**, L338 (1993).

[10] K.P. O'Donnell, *Mater. Res. Soc. Symp.* **595**, W11.26.1 (2000).

[11] C.G. Van de Walle, M.D. McCluskey, C.P. Master, L.T. Romano, N.M. Johnson, *Mater. Sci. Eng. B* **59**, 274 (1999).

[12] M. Bosi, R. Fornari, *J. Cryst. Growth* **265**, 434 (2004).

[13] R.A. Oliver, M.J. Kappers, C.J. Humphreys, G. Andrew, D. Briggs, *J. Appl. Phys.* **97**, 013707 (2005).

[14] N.F. Mott, E.A. Davis, *Electronic Properties in Non-Crystalline Materials*, Clarendon Press, Oxford 1971.

[15] E. Burstein, *Phys. Rev.* **93**, 632 (1954).

[16] T.S. Moss, *Proc. Phys. Soc. Lond. B* **76**, 775 (1954).

[17] M. Kim, J.K. Cho, I.H. Lee, S.J. Park, *Phys. Status Solidi A* **176**, 269 (1999).

[18] M. Ferhat, J. Furthmüller, F. Bechstedt, *Appl. Phys. Lett.* **80**, 1394 (2002).

[19] K.J. Lee, T.S. Oh, K.T. Kim, G.M. Yang, K.Y. Lim, *Phys. Status Solidi C* **3**, 1412 (2006).

[20] J.D. Beach, H.A. Thani, S. McCray, R.T. Collins, J.A. Turner, *J. Appl. Phys.* **91**, 5190 (1998).

[21] S. Srinivasan, F. Bertram, A. Bell, F.A. Ponce, S. Tanaka, H. Omiya, Y. Nakagawa, *Appl. Phys. Lett.* **80**, 550 (2002).

[22] W. Shan, W. Walukiewicz, E.E. Haller, B.D. Little, J.J. Song, M.D. McCluskey, N.M. Johnson, Z.C. Feng, M. Schurman, R.A. Stall, *J. Appl. Phys.* **84**, 4452 (1998).

[23] Y.T. Moon, D.J. Kim, K.M. Song, I.H. Lee, M.S. Yi, D.Y. Noh, C.J. Choi, T.Y. Seong, S.J. Park, *Phys. Status Solidi B* **216**, 167 (1999).

[24] G.M. Diaz, K. Stevens, A. Schwartzman, R. Beresford, *J. Cryst. Growth* **178**, 44 (1997).

[25] A.F. Qasrawi, A.M.M. Shukri, *Cryst. Res. Technol.* **41**, 364 (2006).

[26] J.I. Pankove, *Optical Proccesses in Semiconductors*, Prentice-Hall, New Jersey 1971, p. 93.

[27] C. Sasaki, H. Naito, M. Iwata, H. Kudo, Y. Yamada, T. Taguchi, T. Jyouchi, H. Okagawa, K. Tadatomo, H. Tanaka, *J. Appl. Phys.* **93**, 1642 (2003).

[28] W. Shan, B.D. Little, J.J. Song, Z.C. Feng, M. Schurman, R.A. Stall, *Appl. Phys. Lett.* **69**, 3315 (1996).

[29] T. Takeuchi, S. Sota, M. Katsurgawa, M. Komori, H. Takeuchi, H. Amano, I. Akasaki, *Jpn. J. Appl. Phys.* **36**, L382 (1997).

[30] J.L. Reverchon, F. Huet, M.A. Poisson, J.Y. Duboz, B. Damilano, N. Grandjean, J. Massies, *Mater. Sci. Eng. B* **82**, 197 (2001).